Interacting intersubband excitations in parabolic semiconductor quantum wells

I. K. Marmorkos* and S. Das Sarma
Department of Physics, University of Maryland, College Park, Maryland 20742
(Received 1 February 1993)

We calculate the finite wave-vector intersubband collective excitation spectra in wide parabolic wells at low two-dimensional electron densities where only the lowest quantum subband is occupied by electrons. We use a self-consistent time-dependent local-density approximation to calculate the linear response of the system, comparing our density-functional results with the noninteracting time-dependent Hartree approximation to estimate the magnitudes of exchange-correlation corrections to the collective-mode dispersion. We predict a qualitatively new phenomenon at low electron densities where, in the presence of exchange-correlation effects, it becomes possible for the collective charge-density excitation (i.e., the intersubband plasmon mode) to lie *below* the intersubband quasiparticle continuum. As the electron density is lowered, the charge-density excitation passes through the intersubband single-particle Landau continuum, eventually going below the intersubband single-particle excitations. In this low-density regime ($0.1-0.2\times10^{11}$ cm^{-2}), the collective and the single-particle intersubband excitations are strongly resonantly coupled, leading to an experimentally observable line-splitting phenomenon in the far-infrared-absorption and inelastic-light-scattering spectra. We calculate the far-infrared-absorption spectra self-consistently and find the interesting result that at a critical density even the long-wavelength intersubband charge-density excitation is Landau damped because it is essentially degenerate with the single-particle excitations. We provide detailed numerical results for the intersubband collective charge- and spin-density excitation spectra and the associated far-infrared-absorption spectra for realistic GaAs/Al_xGa_{1-x}As parabolic quantum-well structures, comparing some of our results with the corresponding results for wide square-well structures. We also provide a theoretical comparison between the self-consistent density-functional theory of intersubband linear response with the corresponding diagrammatic perturbation-theory approach.

I. INTRODUCTION

A. Background

During the past 20 years elementary excitations in two-dimensional electron systems confined near semiconductor surfaces and interfaces have been widely studied[1,2] both theoretically and experimentally. During the 1970s, far-infrared-absorption spectroscopy was used extensively[1] to study electronic excitations in silicon inversion (and accumulation) layers whereas during the last 10 years the focus[2] has been on confined electron layers in GaAs systems. Both far-infrared-absorption spectroscopy and inelastic-resonant-light-scattering spectroscopy have been used extensively to study the elementary excitation spectra in single-layer GaAs heterojunctions and quantum wells as well as in GaAs/Al_xGa_{1-x}As multilayer superlattices. Very recently, there has been substantial interest[3-10] in the optical properties of parabolically confined electron layers in wide GaAs/Al_xGa_{1-x}As quantum wells (where either a variation in the alloy concentration x or an introduction of short-period superlattices within the GaAs layer causes a quadratic variation of the bulk band-gap discontinuity along the growth direction leading to a parabolic one-dimensional external potential confining the electron gas). In this paper, we report on a detailed zero-temperature calculation of the elementary charge-density and spin-density intersubband excitation spectra in parabolic quantum wells in the extreme quantum limit, i.e., when only the lowest subband is populated by the electrons. For the sake of comparison and completeness, we also provide some results for the corresponding excitation spectra in more well-studied square quantum-well structures. All our calculations employ experimentally realistic system parameters for GaAs/Al_xGa_{1-x}As quantum-well structures.

In the presence of a confinement potential along the z direction (throughout this paper, we take the x-y plane to be the plane of confinement of the two-dimensional electron gas), which is parabolic for the systems of our interest, the elementary excitations of the system can be divided into intrasubband modes for motion along the x-y plane and intersubband modes for motion along the z direction. This separation of the elementary excitation spectra of the confined system into intrasubband and intersubband modes is, in general, strictly valid[11] only in the long-wavelength limit. The distinction remains approximately valid, however, even at finite (but, not too large) wave vectors because the coupling between the two types of excitations is, in general, small[11] in nonresonant situations. In a symmetric well, however, the coupling between intrasubband and intersubband excitations vanishes[12] as can easily be seen from parity considerations. We consider only intersubband elementary excitations in this paper neglecting all effects of intrasubband (i.e., purely two-dimensional) excitations. We also ignore the coupling[13] of the electronic collective modes to the LO phonons of the system which is allowed because the cal-

culated energies of the intersubband modes we are interested in are substantially lower than the LO-phonon energies of GaAs (or $Al_xGa_{1-x}As$) and, therefore, plasmon-LO-phonon coupling effects are negligibly small. We also uncritically assume the effective-mass approximation (with isotropic parabolic subbands) throughout this work which is, in fact, well valid for the conduction-band electrons in GaAs quantum wells.

There are three different types of intersubband elementary excitations in the quantum wells of interest to us: Single-particle electron-hole excitations (also referred to as quasiparticle excitations), collective charge-density excitations (i.e., intersubband plasmons), and collective spin-density excitations. The single-particle excitations have ($\hbar=1$) energies equal to the subband energy differences,

$$E_{ji}(q)=E_j(\mathbf{k}+\mathbf{q})-E_i(\mathbf{k})=E_{ji}+\frac{q^2}{2m}+\frac{\mathbf{k}\cdot\mathbf{q}}{m}\ , \quad (1.1)$$

where $E_{ji}=E_j-E_i$ is the subband energy difference, and, $\mathbf{k},\mathbf{q}$ are conserved two-dimensional wave vectors in the x-y plane of confinement. At zero temperature, the wave vector $k=|\mathbf{k}|$ must be less than k_F where k_F is the Fermi wave vector in the occupied ground subband, and, therefore, the Landau continuum of single-particle intersubband excitations between the ground subband $i\equiv 0$ and an excited subband $j\equiv n$ is bounded by the parabolas $E_{n0}+q^2/2m+k_Fq/m$ and $E_{n0}+q^2/2m-k_Fq/m$. In this paper, we are interested in intersubband transitions between the occupied ground subband 0 and the first excited subband $n=1$ which leads to the lowest intersubband transitions $E_{10}(q)$. In the presence of many-body effects, the energies (and effective masses) should correspond to quasiparticles rather than noninteracting electrons. The single-particle excitations are, therefore, by definition at the single-particle energy differences between the subbands.

The collective charge-density excitations are the intersubband plasmon modes of the confined electron layer and, as such, are associated with the *reducible* response function of the system. The collective spin-density excitations, which can be probed by inelastic-light-scattering spectroscopy, occur at the poles of the *irreducible* response functions of the system. As is obvious from its definition, the single-particle excitations arise from the leading-order intersubband polarizability diagram [Fig. 1(a)] where the vertex correction associated with the excitonic interaction between the electron in the excited subband and the hole in the ground subband is ignored. The exchange-correlation corrections to individual subbands is included, however, through the renormalized Green's function for each subband as shown in Figs. 1(b) and 1(c). The spin-density collective modes are the poles of the irreducible response function [Fig. 1(d)] where the vertex correction [Fig. 1(e)] incorporates the effective excitonic interaction. The reducible response function [Fig. 1(f)], whose poles give the charge-density excitations, is formed by dynamically screening the irreducible response function through the infinite series of ring diagrams.

While the many-body diagrams (Fig. 1) defining the intersubband elementary excitations are conceptually and formally quite simple, carrying out a real calculation within the Feynman-Dyson many-body perturbation scheme of Fig. 1 is exceedingly difficult if one has to include the exchange-correlation-induced self-energy corrections in the calculation. While the many-body intersubband quasiparticle excitation energies have been calculated[14,15] for silicon inversion layer systems (and for the ground subband of GaAs structures) within the leading-order dynamically screened GW approximation, no theoretically consistent calculation of the intersubband response functions which goes beyond the simple random-phase approximation (RPA) really exists. There have been some attempts[16–18] at including vertex corrections in the theory by calculating the ladder-bubble diagrams approximately, but in our opinion no satisfactory

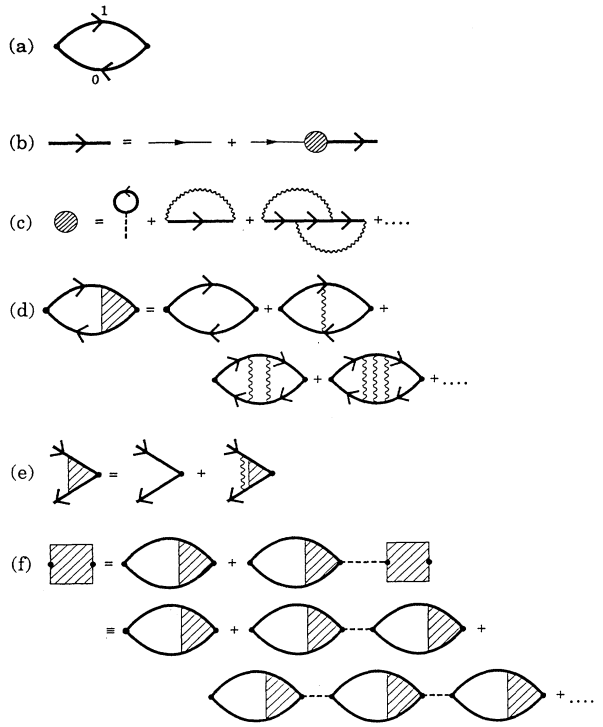

FIG. 1. Many-body diagrams for the intersubband elementary excitations: (a) the intersubband leading-order polarizability (gives the quasiparticle continuum); (b) the renormalized subband Green's function with the thin line being bare Green's function; (c) the self-energy with the leading contributions coming from the Hartree "tadpole" diagram, the "GW" diagram, and the "$GW\Gamma$" diagram including the first-order vertex correction; (d) the interacting irreducible intersubband polarizability (gives the collective spin-density excitations) and the ladder series of vertex corrections; (e) the ladder integral equation for the vertex function; and (f) the reducible intersubband polarizability (gives the collective charge-density excitations) as sum of the ring diagrams. The dashed and the wiggly lines are the (unscreened) direct intersubband Coulomb interaction, and the (dynamically screened) exchange-correlation interaction, respectively. (In the TDLDA, one approximates the wiggly line as a static, local interaction.) In the RPA, one neglects all vertex corrections [i.e., uses (a) for the irreducible polarizability] and includes only the Hartree self-energy diagram [the first diagram, the tadpole, in (c)].

diagrammatic evaluation of intersubband response beyond RPA has been carried out because all the existing calculations[16–18] involving intersubband vertex corrections neglect self-consistency in the wave functions.

The most widely used technique[9,19–21] for calculating intersubband response in confined semiconductor structures has been the self-consistent local-density-functional theory where the subband energies and wave functions are calculated by self-consistently solving Poisson's equation and the one-electron Schrödinger-like Kohn-Sham equation of the density-functional theory with the exchange-correlation potential approximated in the local-density approximation (LDA). The intersubband response functions can then be calculated in a linear-response calculation using the self-consistent LDA subband wave functions and energies. This self-consistently coupled linear-response LDA calculation can be referred to as the time-dependent local-density approximation (TDLDA) in the same spirit of the RPA being the time-dependent Hartree approximation. This (i.e., the TDLDA) is the main technique we adopt throughout this paper for our calculation of finite wave-vector intersubband response in realistic parabolic quantum wells. We also provide some representative diagrammatic RPA (and, Hubband approximation) results for the purpose of comparison between diagrammatic and TDLDA calculations.

There has been a great deal of recent interest[3–10] in the optical properties of parabolic quantum wells. A particularly significant aspect[8] of parabolic systems is that at long wavelengths optical absorption is unaffected by electron interaction effects and occurs[3] only at the bare simple harmonic frequency of the unperturbed well. This exact result (for a perfectly parabolic system) asserting that the long-wavelength charge-density collective mode is the same as the bare subband energy difference is a generalized version of Kohn's theorem which states that in an electron gas within a jellium model the long-wavelength cyclotron resonance is unaffected by electron-electron interaction effects. The experimental $GaAs/Al_xGa_{1-x}As$ parabolic quantum-well systems are, of course, not perfectly parabolic systems. But, it turns out that they obey[3–7] the generalized Kohn's theorem very well (better than 1%) and, in fact, the insensitivity of the long-wavelength magneto-optical absorption frequency in parabolic wells to the electron density in the system is well established experimentally. Thus, exchange-correlation many-body corrections do not affect the long-wavelength intersubband charge-density collective mode in parabolic wells. It therefore becomes an interesting issue to investigate the extent to which exchange and correlation corrections affect the finite wave-vector energy dispersion of charge-density collective modes in parabolic wells. A complementary issue, the exchange-correlation correction to the *long-wavelength* intersubband charge-density excitation in *realistic* (i.e., imperfect) parabolic wells, has recently been investigated[9] theoretically. In this paper, our goal is to extend the calculation to finite wave vectors and also to compare the results for the parabolic well with those for the square well.

The insensitivity of the long-wavelength optical transition energy to electron-electron interaction effects in a parabolic well[3,8] is based on the simple fact that a parabolic confining potential allows the separation of the many-body Hamiltonian into center of mass and relative coordinates with the electron-electron interaction term depending only on the relative coordinates. Since the long-wavelength (i.e., $q=0$) external radiation can couple only to the center-of-mass coordinates, the long-wavelength response of the many-body interacting parabolic system is exactly the same as that of the bare system (i.e., with only one electron in the well), and the collective charge-density excitation energy at $q=0$ is the bare harmonic-oscillator energy. This exact theorem, while being quite useful in checking the numerical accuracy of a particular computational scheme, is not helpful in determining the exchange-correlation corrections to the intersubband charge-density excitation energy at *finite q* where the many-body Hamiltonian is not separable into center of mass and relative coordinates (due to the broken translational invariance associated with finite q) and, therefore, the collective mode is affected by exchange and correlation. One of our goals in this paper is to calculate quantitatively the full wave-vector-dependent dispersion of the intersubband charge-density excitation. Not unexpectedly, we find that at finite q the intersubband charge-density mode in parabolic wells is significantly affected by electron interaction effects, and the exchange-correlation correction is comparable to that in square-well systems (where no generalized Kohn's theorem applies even at $q=0$). We emphasize that most of our calculations are for experimentally realistic $GaAs/Al_xGa_{1-x}As$ parabolic wells, and not for ideal infinite parabolic wells (to which the Kohn's theorem applies rigorously).

We also explore the generic issue of the extent of exchange-correlation corrections on the collective intersubband mode dispersion in semiconductor quantum wells. There has not been any detailed general theoretical study of this subject. We concentrate on low two-dimensional electron densities in most of our calculations because it is well known that exchange-correlation effects are relatively less important in GaAs systems at higher two-dimensional densities (above 10^{11} cm^2). We find that at low densities there are significant deviations in our TDLDA-calculated collective-mode dispersion compared with the RPA results, showing that exchange-correlation corrections on the intersubband collective-mode dispersion can be substantial.

Some remarks about notations and units are in order before we discuss our calculations. We take $\hbar=1$ throughout this paper. All wave vectors (denoted mainly by $\mathbf{q}$ or $\mathbf{k}$) are conserved two-dimensional wave vectors in the plane of confinement of the electron layer. The electron gas has a two-dimensional electron density of N_S per unit area, with all the electrons occupying only the ground subband of the system. The quantities E_F and k_F denote the two-dimensional Fermi energy and Fermi wave vector, respectively, in the ground subband. The bare parabolic well is characterized by a simple harmonic frequency ω_0 which is, by definition, also the bare subband separation before the inclusion of electron interaction effects. The curvature of the well ω_0 is related to the

potential height Δ and the width W of the well via the relationship

$$\omega_0=\left[\frac{8\Delta}{mW^2}\right]^{1/2} .$$

In the density-functional calculations (Secs. II–IV) we find it convenient to express the two-dimensional density in the units of the usual dimensionless r_s parameter where the length is measured in units of the effective two-dimensional Bohr radius $a_B=\epsilon_0\hbar^2/2me^2$, where ϵ_0 is the lattice dielectric constant. In our density-functional calculations (Secs. II–IV) we express energy (or frequency) in atomic units with the energy measured in effective Ry$=e^2/2a_B$. For GaAs/$Al_xGa_{1-x}As$ structures 1 Ry$\equiv$5.8 meV and $a_B\equiv$98.7 Å.

The rest of this paper is organized as follows. In Secs. I B and I C we briefly discuss a many-body diagrammatic perturbation approach to calculating the collective intersubband modes, pointing out the difficulty of including the exchange-correlation effects within the diagrammatic approach. In Secs. II–IV we describe our TDLDA theory for intersubband response and present self-consistent density-functional numerical results for collective spin-density and charge-density intersubband excitations. We conclude in Sec. V with a brief summary.

B. Diagrammatic RPA

The simplest possible approximation is to neglect all vertex corrections to the irreducible response function so that the irreducible intersubband polarizability is given by the bare bubble. Within this approximation scheme, the single-particle excitations and the collective spin-density excitations are identical. The intersubband collective charge-density excitations are obtained by summing all the intersubband bubble (or the ring) diagrams where the Hartree self-energy shift for each subband must be included in each individual subband Green's function to preserve the Ward identity (and current conservation). This is the diagrammatic version of RPA which is just the time-dependent Hartree approximation.

For the two-subband model, where we concentrate on the optical transitions between the occupied ground subband (0) and the first excited subband (1), the collective charge-density excitations are given by the poles of the reducible intersubband polarizability function which is the geometric series formed by the irreducible intersubband bubble diagrams. Equivalently, the collective charge-density excitations are given by the zeros of the intersubband dielectric function $\epsilon_{10}(q,\omega)$,

$$\epsilon_{10}(q,\omega)=1-V_{0101}(q)P_{10}(q,\omega)=0 , \tag{1.2}$$

where the irreducible intersubband polarizability function $P_{10}(q,\omega)$ is given by ($\hbar=1$)

$$P_{10}(q,\omega)=\frac{m}{\pi}\frac{k_F}{q}(a_- -a_+ +\sqrt{a_+^2-1}-\sqrt{a_-^2-1}) , \tag{1.3}$$

$$a_\pm=\frac{\omega\pm(\omega_0+\Sigma_1^{\rm dir}-\Sigma_0^{\rm dir})}{qv_F}\pm\frac{q}{2k_F} , \tag{1.4}$$

with $\Sigma_{1,0}^{\rm dir}$ being the Hartree, or the direct Coulomb self-energy corrections to the two subbands (which are nonzero in this problem only by virtue of the broken translational invariance in the z direction). The quantity ω_0 in Eq. (1.4) above is the bare subband separation $\omega_0=E_1-E_0$ of the empty parabolic well or, equivalently, ω_0 is the simple harmonic frequency of the parabolic confining potential $V_p(z)=\frac{1}{2}m\omega_0^2z^2$.

The matrix element $V_{1010}(q)$ is the intersubband Coulomb interaction matrix element which for purely parabolic confinement is given, in general, by

$$V_{\alpha\beta\gamma\delta}(q)=\frac{2\pi e^2}{\epsilon_\infty q}\int dz\int dz'\phi_\alpha(z)\phi_\beta(z')\phi_\gamma(z')\phi_\delta(z)e^{-q|z-z'|}$$
$$=\frac{2e^2}{\epsilon_\infty}\left[\frac{2^{\alpha+\beta}\gamma!\delta!}{2^{\gamma+\beta}\alpha!\beta!}\right]^{1/2}\left[\frac{il}{2}\right]^{\alpha-\delta+\beta-\gamma}(-1)^{\beta-\gamma}\int_{-\infty}^{+\infty}dx\frac{x^{\alpha-\delta+\beta-\gamma}}{x^2+q^2}e^{-x^2l^2/2}L_\delta^{\alpha-\delta}\left[\frac{x^2l^2}{2}\right]L_\gamma^{\beta-\gamma}\left[\frac{x^2l^2}{2}\right] , \tag{1.5}$$

where L is the associated Laguerre polynomial, and α, β, γ, δ are subband indices, $l^2=(1/m\omega_0)$, and ϵ_∞ is the background dielectric constant. [$\phi_\alpha(z)$, etc. are the subband wave functions which for the parabolic potential case are the simple harmonic-oscillator eigenfunctions and $(2\pi e^2/\epsilon_\infty q)e^{-q|z-z'|}$ is the two-dimensional Fourier transform of the Coulomb interaction.]

Before presenting our numerical results for the intersubband charge-density mode dispersion based on the solution of Eq. (1.2), we make a few remarks regarding the diagrammatic RPA calculation. (1) The intrasubband and intersubband charge-density excitations are totally decoupled even at finite wave vectors for the symmetric parabolic potential well. This is true for all symmetric potentials where the single-particle subband wave functions are parity eigenstates leading to the vanishing of the Coulomb matrix element that couples intrasubband and intersubband excitations. (2) Doing a straightforward long-wavelength expansion of $P_{10}(q,\omega)$ and $V_{1010}(q)$ in Eq. (1.2) it is possible to show (after some algebra) that the intersubband charge-density dispersion, up to $O(q^2)$, is given by

$$\omega_p^2=(\omega_{10}^2+2N_S\omega_{10}a_0)-2N_S\omega_{10}a_1q$$
$$+\left[2N_S\omega_{10}a_2+\frac{\omega_{10}+N_Sa_0}{m}+\frac{2\pi(2\omega_{10}+3N_Sa_0)}{4m^2a_0}\right]$$
$$\times q^2+O(q^3) , \tag{1.6}$$

where N_S is the two-dimensional electron density in the system, ω_{10} is the subband energy separation including the Hartree self-energy corrections, i.e.,

$$\omega_{10}=\omega_0+\Sigma_1^{\rm dir}-\Sigma_0^{\rm dir}\ , \tag{1.7}$$

and the positive definite quantities a_n's in Eq. (1.6) are the expansion coefficients of $V_{1010}(q)$ in powers of q,

$$V_{1010}(q)=a_0-a_1q+a_2q^2-a_3q^3+\cdots\ , \tag{1.8}$$

with

$$a_n=\frac{4\pi e^2}{\varepsilon_\infty}\frac{1}{n!}\int_0^\infty dz\phi_0(z)\phi_1(z) \times\int_0^\infty dz'\phi_0(z')\phi_1(z') \times(|z+z'|^{n+1}-|z-z'|^{n-1})\ . \tag{1.9}$$

The first two terms (within parentheses) in Eq. (1.6) combine to produce the generalized Kohn's theorem result $\omega_{10}^2+2N_S\omega_{10}a_0=\omega_0^2$, which is exact for the perfectly parabolic well (and is an extremely good approximation for real parabolic wells). Note that ω_{10} $(=\omega_0+\Sigma_1^{\rm dir}-\Sigma_0^{\rm dir})$ is actually well below ω_0 because $\Sigma_0^{\rm dir}$ is substantially larger than $\Sigma_1^{\rm dir}$, but the depolarization shift term $2N_S\omega_{10}a_0$ arising from resonance screening associated with the sum of all the intersubband ring diagrams brings the long-wavelength intersubband charge-density frequency back to the bare frequency ω_0. The direct self-energy correction exactly cancels the depolarization shift correction in a parabolic well. Thus, the generalized Kohn's theorem holds in every order of perturbation theory provided the self-energy and the polarization diagrams are consistent with each other (i.e., they satisfy the Ward identity). Thus, RPA response calculation demands that the single-particle Green's function be calculated in the self-consistent Hartree approximation. There have been earlier analytical calculations leading to results similar to our Eq. (1.6), but these results neglected Hartree self-energy corrections and are, therefore, not current conserving. For parabolic confinement, use of the RPA without the Hartree correction will lead to a violation of the generalized Kohn's theorem. A second point to note about Eq. (1.6) is that it predicts a negative long-wavelength dispersion for the intersubband charge-density excitation mode arising from the negative linear-q term. In fact, Eq. (1.6) predicts that the intersubband collective charge-density excitation mode has an energy minimum at a finite value of the wave vector. (3) The single-particle Green's function entering the RPA calculation should be the *self-consistent* Hartree Green's functions and, thus, in addition to renormalizing the bare subband energies by the direct self-energy correction, we should also renormalize the wave functions (in calculating, for example, the Coulomb matrix elements) and use the self-consistent Hartree wave function in our calculation. In the spirit of the leading-order perturbation theory, we have used the bare (simple harmonic oscillator) wave functions in our numerical calculations of Eq. (1.2) presented below, finding that this is adequate to preserve the generalized Kohn's theorem to better than 1% relative accuracy which is sufficient for our purpose.

In Fig. 2 we show the numerically calculated [by directly solving Eq. (1.2)] RPA intersubband collective charge-density excitation dispersion for an infinite parabolic well system with $r_s=10$ and $\omega_0/E_F=6.0$. (These parameters correspond to a fairly typical wide parabolic well which has a potential height of 150 meV at a width of 4100 Å.) For other values of ω_0, we get similar qualitative behavior. In the inset of Fig. 2 we show the calculated dispersion for $r_s=4.3$. The generalized Kohn's theorem is obeyed to better than 1% in these numerical RPA results and the finite wave-vector minimum in the dispersion, while being shallow, is clearly visible in both the results. The finite wave-vector dispersion minima in the collective intersubband charge-density mode arise from an interplay between confinement and nonlocal effects which makes the leading-order correction to the collective-mode energy negative. Note that this intersubband minimum, already showing up in RPA, is not a many-body effect and is related to similar negative dispersion shown by surface-plasmon modes in metals. While the negative dispersion in metallic surface plasmons has been experimentally seen, we do not know of any direct experimental observation of the dispersion minima in intersubband collective charge-density excitations in quantum wells. The minimum decreases in size (and moves to lower wave vectors) as the electron density is decreased. It also goes down with increasing ω_0. This minimum, being extremely shallow, may be difficult to detect experimentally.

C. Going beyond RPA

As emphasized earlier, going beyond RPA and including exchange and correlation effects in the intersubband

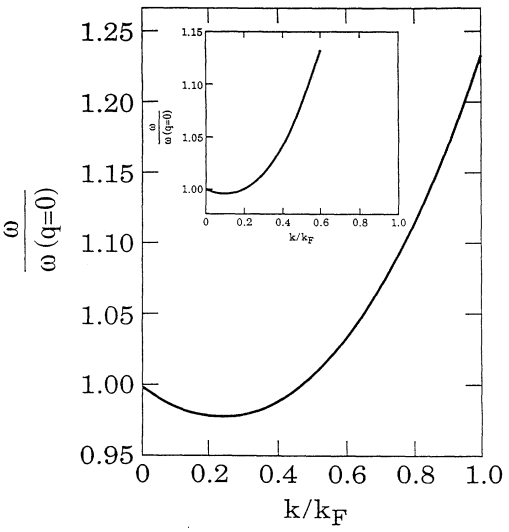

FIG. 2. The lowest intersubband charge-density excitation in a parabolic well within the diagrammatic RPA for $r_s=10$ and $\omega_0=6E_F$. The inset shows the same for $r_s=4.3$. The dispersion is plotted up to the critical wave vector where the collective mode enters the single-particle continuum and becomes damped.

response calculation is very difficult to accomplish diagrammatically. We have carried out two very simple model calculations of intersubband response going beyond RPA within the diagrammatic approach.

One is a simple Hubband approximation to the local-field corrections in the intersubband response. In this approximation scheme, one is solving the ladder vertex integral equation for the irreducible polarizability in a very crude fashion. The intersubband charge-density mode in the Hubbard approximation is formally given by the same equation as in RPA [i.e., Eq. (1.2)],

$$1-V_{0101}(q)P^{H}_{10}(q,\omega)=0 \ , \tag{1.10}$$

where the irreducible polarizability $P^{H}_{10}(q,\omega)$ is related to the corresponding bare polarizability $P_{10}(q,\omega)$ of the RPA calculation by the formula

$$P^{H}_{10}(q,\omega)=\frac{P_{10}(q,\omega)}{1+V_{0101}(q)G(q)P_{10}(q,\omega)} \ , \tag{1.11}$$

with the local-field correction $G(q)$ approximated by

$$G(q)=\frac{q}{2(q^2+k_F^2)^{1/2}} \ . \tag{1.12}$$

We show our calculated intersubband charge-density mode dispersion within the Hubbard approximation in Fig. 3 using the same parameters as those for the RPA results of Fig. 2. Qualitatively, the Hubbard approximation results are similar to the RPA results except that the dispersion minimum is somewhat deeper. Note that the local-field correction $G(q)$ vanishes in the $q\rightarrow 0$ limit, and, therefore, the generalized Kohn's theorem is preserved in the Hubbard approximation.

We also attempted a many-body calculation by including the Hartree-Fock exchange self-energy in our calculation. A non-self-consistent Hartree-Fock calculation using the full Coulomb interaction in the exchange self-energy, however, led to a rather strong violation (by about 10–20 %) of the generalized Kohn's theorem, making suspect similar calculations[17,18] carried out in the context of other systems. Another model calculation where we approximate the electron-electron interaction entering the exchange self-energy diagram and the corresponding ladder vertex diagrams by a short-ranged static interaction led to results very close to the Hubbard-approximation results. This is not surprising because the Hubbard approximation is essentially an approximate solution of the ladder vertex equation where the wave-vector dependence of the three-point vertex function is approximated by a static short-range local interaction.

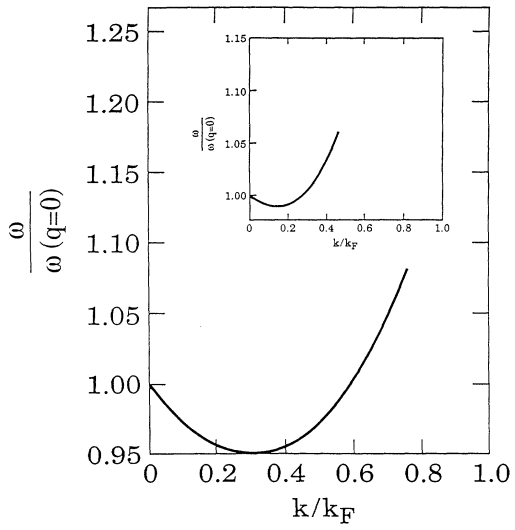

FIG. 3. The same as in Fig. 2 for the diagrammatic Hubbard approximation as explained in the text.

Clearly, a computationally efficient diagrammatic many-body calculation which can include exchange-correlation effects in the theory of intersubband response has not yet been developed. It is, indeed, a very difficult task because it involves solving a set of coupled integral equations (Fig. 1) involving both wave-vector and frequency integrations. We therefore turn to the density-functional TDLDA theory which is discussed in Secs. II–IV.

II. SELF-CONSISTENT LOCAL-DENSITY-FUNCTIONAL THEORY

A. Electronic structure

Before we present our theory of intersubband response and optical absorption in a quantum well, it is instructive to highlight first some of the technical aspects of the method used to calculate self-consistently the electronic structure of a quantum well.

In the density-functional theory, an electron is assumed to move in an effective potential,

$$V_{\rm ef}(z)=V_p(z)+V_H(z)+V_{\rm xc}(z) \ , \tag{2.1}$$

where $V_p(z)$ determines the shape of the confining quantum-well potential, $V_H(z)$ is the electrostatic Hartree potential due to the average charge density of the other electrons in the well, and $V_{\rm xc}(z)$ describes exchange and correlation effects in the density-functional formalism due to Hohenberg, Kohn, and Sham. The exchange-correlation potential energy is, in general, an unknown functional $V_{\rm xc}[n(z)]$ of the electron density $n(z)$. In practice, however, the simplest and most widely used approximation to $V_{\rm xc}(z)$ is the so-called local-density approximation (LDA). In this approximation, one replaces the functional $V_{\rm xc}[n(z)]$ with a function $V_{\rm xc}[n(z)]=\mu_{\rm xc}[n_0=n(z)]$, where $\mu_{\rm xc}$ is the exchange correlation contribution of the chemical potential of a homogeneous electron gas of density n_0 equal to the local electron density $n(z)$ of the inhomogeneous system. LDA has been found to work surprisingly well in calculating the electronic structure of confined electronic systems. There are many good reviews of this technique, and we refer the reader to them for further details.[22] The exchange-correlation potential $V_{\rm xc}$ for LDA has been parametrized by several authors and in our work we adopt a standard parametrized form[23] originally due to Hedin and Lundqvist,

$$V_{xc}(z)=-\left[1+0.7734x\ln\left[1+\frac{1}{x}\right]\right]\left[\frac{2}{\pi\alpha r_s}\right], \quad (2.2)$$

where $\alpha=(4/9\pi)^{1/3}$, $x=x(z)=r_s/21$, and

$$r_s=r_s(z)=[\tfrac{4}{3}\pi\alpha_B^3 n(z)]^{1/3}. \quad (2.3)$$

(The exchange-correlation potential above is given in units of the effective Rydberg.) This form for V_{xc} has been very successful[24] in calculating the electronic structure of GaAs/AlAs heterojunctions.

We assume the effective-mass approximation and consider the electron effective mass m to be constant throughout the quantum well. This allows the z-dependent degrees of freedom to be decoupled from the ones in the x-y plane (where the electron motion is assumed to be free). In this case, the electronic subband wave functions $\zeta_n(z)$ and the quasiparticle energies E_n for the nth subband are identified with the solutions of the Kohn-Sham equation,[25]

$$\left[-\frac{\hbar^2}{2m}\frac{d^2}{dz^2}+V_{ef}(z)\right]\zeta_n(z)=E_n\zeta_n(z). \quad (2.4)$$

Equation (2.4) is formally the same as Schrödinger's equation in the Hartree approximation, but now the potential energy $V_{ef}(z)$ includes also exchange and correlation effects through $V_{xc}(z)$ in the LDA approximation.

The Hartree potential energy $V_H(z)$ satisfies Poisson's equation,

$$\frac{d^2V_H(z)}{dz^2}=-\frac{4\pi e^2}{\varepsilon_0}[n(z)-n_I(z)], \quad (2.5)$$

where $n_I(z)$ is the density of the positively charged donor impurities producing the electron gas, and $n(z)$ is the z-dependent electron density determined from the subband wave functions through

$$n(z)=2\sum_{n}^{n_{max}} N_n|\zeta_n(z)|^2, \quad (2.6)$$

with n_{max} is the highest occupied subband in the system, N_n is the occupancy of the nth subband and the factor of 2 coming from spin. (In all our calculations the total electron density is low enough so that only the ground subband is occupied.)

In our calculation we concentrate on a truncated parabolic quantum well given by

$$V_p(z)=\alpha z^2\theta\left[\frac{W}{2}-|z|\right]+V_0\theta\left[|z|-\frac{W}{2}\right], \quad (2.7)$$

where α is the curvature of the parabolic well given by $\alpha=4\Delta/W^2$, with Δ the height of the parabolic portion of the well at the edge of the well. V_0 is the barrier height above the edge of the parabolic portion (Fig. 4). In Fig. 4 we show the typical results for a wide parabolic well of width $W=1600$ Å, $\Delta=150$ meV, and $V_0=130$ meV. We see that for an electron density of $N_S=1.1\times10^{11}$ cm^{-2} the renormalization of the well is quite substantial. All our density-functional calculations are based on finite parabolic wells of the type shown in Fig. 4. In the calculations described in the rest of this paper, the subband energies and wave functions are those obtained by a self-consistent solution of Eqs. (2.1)–(2.7).

B. Collective intersubband modes in the TDLDA theory

By definition, the single-particle intersubband spectrum for transitions between the ground ($n=0$) and the first excited ($n=1$) subband is given by ($\hbar=2m=1$)

$$E_{10}(\mathbf{k},\mathbf{q})=E_1(\mathbf{k}+\mathbf{q})-E_0(\mathbf{k})=E_{10}+q^2+2\mathbf{k}\cdot\mathbf{q},$$

where $E_{10}=E_1-E_0$ is the energy difference between the LDA calculated subband bottoms. For each value of $q=|\mathbf{q}|$, $E_{10}(\mathbf{k},\mathbf{q})$ denotes a continuum of single-particle transitions (the so-called intersubband Landau continuum) bounded by the parabolas $E_{10}+q^2-2k_Fq$ and $E_{10}+q^2+2k_Fq$. When an intersubband collective mode enters the Landau continuum, it becomes damped due to the emission of electron-hole pairs and loses its coherent collective character. In our theory, which neglects multiple electron-hole pair emission, the collective modes are undamped (except for a small collisional damping by impurities) outside the single-particle Landau continuum.

There are a number of equivalent ways of obtaining the intersubband collective modes in the density-functional theory within the LDA. The conceptually easiest is perhaps to note that in the LDA, the effective exchange-correlation interaction is approximated by a local (i.e., q-independent) and static (i.e., ω-independent) interaction V_{xc} which provides the self-energy correction for the individual subbands through the self-consistent calculation and must, therefore, be included in the intersubband response calculation as a static and q-independent vertex correction given by the matrix element U_{xc}^{1010},

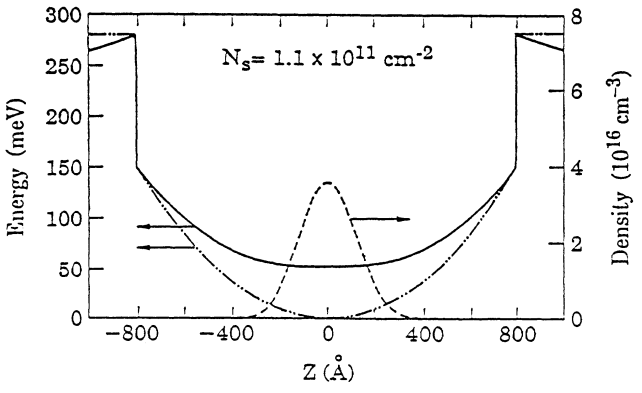

FIG. 4. Calculated potential and charge-density profile in a parabolic quantum well. Solid curve shows the self-consistently calculated potential of the well, dashed-dot-dot curve corresponds to the potential of the bare, empty well, and the dashed one represents the self-consistent charge-density profile for an electron density of $N_S=1.1\times10^{11}$ cm^{-2}.

$$U_{xc}^{1010}=\left|\int dz\int dz'\zeta_1(z)\zeta_0(z)\times\frac{\partial V_{xc}}{\partial n(z)}\delta(z-z')\zeta_1(z')\zeta_0(z')\right|$$
$$\equiv\left|\int dz|\zeta_1(z)|^2|\zeta_0(z)|^2\frac{\partial V_{xc}}{\partial n(z)}\right| . \quad (2.8)$$

The inclusion of a static q-independent ladder vertex correction in the intersubband polarizability is easy to carry out. The vertex integral equation for the irreducible polarizability $\tilde{P}_{10}(q,\omega)$ within this simple LDA ladder approximation forms a geometric series which is easily solved to give

$$\tilde{P}_{10}(q,\omega)=\frac{P_{10}(q,\omega)}{1+U_{xc}^{1010}P_{10}(q,\omega)} , \quad (2.9)$$

where $P_{10}(q,\omega)$ is the leading-order intersubband polarizability bubble (with no vertex correction) given by the same equation as Eq. (1.4) except that the subband energies entering $P_{10}(q,\omega)$ are the LDA subband energies which include exchange-correlation corrections in addition to the Hartree corrections.

The reducible polarizability function is formed as usual by summing the infinite series of ring diagrams to give

$$\tilde{P}_{10}^{(R)}=\frac{\tilde{P}_{10}(q,\omega)}{1-V_{1010}(q)\tilde{P}_{10}(q,\omega)} , \quad (2.10)$$

where $V_{1010}(q)$ is, as before, the matrix element of the Coulomb interaction $(2\pi e^2/\varepsilon_\infty q)e^{-q|z-z'|}$ between the LDA subband wave functions. Using (2.9) in (2.10) we get

$$\tilde{P}_{10}^{(R)}(q,\omega)=\frac{P_{10}(q,\omega)}{1-(V_{1010}(q)-U_{xc}^{1010})P_{10}(q,\omega)} . \quad (2.11)$$

The poles of the response function P_{10}, $\tilde{P}_{10}$, and, $\tilde{P}_{10}^{(R)}$ define, respectively, the single-particle excitations, the collective spin-density excitations, and the collective charge-density excitations for the intersubband transitions between the lowest ground subband and the first excited subband.

Thus, the dispersion of the collective intersubband spin-density and charge-density excitation modes are given, respectively, by the following equations in TDLDA:

$$1+U_{xc}^{1010}P_{10}(q,\omega)=0 , \quad (2.12)$$

and

$$1-[V_{1010}(q)-U_{xxc}^{1010}]P_{10}(q,\omega)=0 . \quad (2.13)$$

Note that if we put $V_{xc}\equiv 0$ which, in turn, makes $U_{xc}^{1010}=0$, our theory becomes the time-dependent Hartree theory which is exactly the same as the diagrammatic RPA discussed in Sec. I (except that the wave functions are self-consistent Hartree wave functions in the current case). Note that within the time-dependent Hartree theory, there are no collective spin-density excitations distinct from the single-particle excitations because $\tilde{P}_{10}(q,\omega)\equiv P_{10}(q,\omega)$ in the absence of vertex corrections.

So far, we have only considered a two-subband model in discussing intersubband collective-mode dispersion (because all our numerical results are for this situation). But a generalization to multisubband case is formally straightforward by interpreting various quantities entering the above equations as matrices. Thus, the intersubband spin- and charge-density collective modes are given, respectively, by the following determinantal equations in the multisubband situation:

$$|1+U_{xc}P|=0 , \quad (2.14)$$

and,

$$|1-(V-U_{xc})P|=0 , \quad (2.15)$$

where 1 is the unit matrix, and, P, V, U_{xc} are, respectively, the matrices representing the leading-order polarizability, the Coulomb interaction, and the exchange-correlation vertex correction. We mention that, instead of using the diagrammatic many-body approach adopted here, one can also derive the formal equations for intersubband collective-mode dispersion by using the equation of motion for the density matrix in the self-consistent-field approach[26] of Ehrenreich and Cohen, or, equivalently, by using a time-dependent perturbation calculation[19] as was done by Ando. We believe that our diagrammatically inspired ladder vertex equation approach is conceptually the simplest technique at obtaining the collective-mode dispersion.

We conclude this section by pointing out that the dynamical structure factors defined by $\mathrm{Im}\tilde{P}$ and $\mathrm{Im}\tilde{P}^{(R)}$ define, respectively, the inelastic-light-scattering intensity of the spin-density and the charge-density excitation spectra. Noting that we can write $\tilde{P}^{(R)}\equiv\varepsilon^{-1}\tilde{P}$ where $\varepsilon=1-(V-U_{xc})\tilde{P}$, we can identify ε as the intersubband dielectric matrix for the system. If the exchange-correlation-induced self-energy and vertex corrections are neglected by putting V_{xc} and U_{xc} to be zero, we get the usual RPA dielectric function $\varepsilon=1-V\tilde{P}$.

The preferred experimental technique[3-7] for studying the optical properties of parabolic quantum wells has been the far-infrared-absorption spectroscopy. We, therefore, develop a theory for the finite wave-vector optical absorption in the parabolic wells in the next section before presenting our numerical results.

III. THEORY OF OPTICAL ABSORPTION IN A QUANTUM WELL

In this section we develop a theory for the intersubband optical absorption at finite wave vectors in a quantum well. As we mentioned in Sec. I, the peaks of the absorption correspond to the collective charge-density modes of the system and, consequently, must be determined from the poles of the appropriate response function. Our main goal is to calculate the conductivity of the electron gas at finite wave vectors and then look for its poles. In our theory, we are going to incorporate resonance screening (sum of the ring diagrams) effects and excitonic vertex corrections in the LDA approximation.

We use self-consistent single-particle wave functions and quasiparticle energies that include exchange and correlation effects, as described in Sec. II.

Intersubband optical absorption of a confined electron gas has been studied theoretically[9,19–21] in the past by a number of authors mainly in the limit of zero wave vector. Ando reported[19] a theory of optical absorption of an electron gas in space-charge layers on semiconductor surfaces by taking into account exchange and correlation effects in the LDA approximation. We generalize Ando's absorption calculation[19] to finite wave vectors, and recover his results in the limit of zero wave vector.

In our model we consider an electron gas in a quantum well (e.g., parabolic, or square) of total areal density N_S. Intersubband transitions correspond to motion of the confined electrons along the direction of the confinement (taken to be the z axis). Such transitions, therefore, can couple only to the component of the electric field of the radiation perpendicular to the electronic sheet. At zero wave vector, this is the only way the charge in the well can absorb infrared radiation (we neglect scattering of the electrons by impurities and phonons). Because we are interested in the intersubband optical absorption we take the electric field D of the radiation to be polarized along the z axis. We use the dipole approximation in describing the interaction between the external radiation and the electrons, and neglect retardation effects. This is a good approximation since the thickness of a typical quantum well is much smaller than the wavelength of the light with frequency resonant with the self-consistent subband separation in the well. We assume the external perturbation (radiation field) is given by

$$De^{i\mathbf{q}\cdot\mathbf{r}-i\omega t} . \tag{3.1}$$

The vectors $\mathbf{q}$ and $\mathbf{r}$ are in the x-y plane of the electronic sheet. The external perturbation modifies the density distribution of electrons, and, consequently, the Hartree and the exchange-correlation potentials as well. The change of the electron distribution is given by the form

$$\Delta n(q,z)e^{i\mathbf{q}\cdot\mathbf{r}-i\omega t} \tag{3.2}$$

and after applying standard time-dependent perturbation theory we get

$$\Delta n(q,z)=-2N_S\sum_{n>0}\zeta_n(z)\zeta_0(z)\Pi_n(q,\omega)\langle n|H'(q)|0\rangle . \tag{3.3}$$

In the above, we consider only the lowest subband populated in the ground state and study transitions to excited levels n. In Eq. (3.3) we have

$$\Pi_n(q,\omega)=\frac{1}{N_S}\int\frac{d^2k}{(2\pi)^2}f_0(k)\times\left[\frac{1}{\omega-\omega_n(k+q)+i\delta}-\frac{1}{\omega-\omega_n(k-q)+i\delta}\right] , \tag{3.4}$$

with

$$\omega_n(k+q)=E_n(k+q)-E_0(k) , \tag{3.5}$$

$$E_n(k)=E_n+\frac{k^2}{2m} , \tag{3.6}$$

and $f_0(k)$ the Fermi factor. $\Pi_n(q,\omega)$, which is closely related to the polarizability P of Secs. I and II, can be calculated analytically to give

$$\Pi_n(q,\omega)=\frac{m}{2\pi N_S}\frac{k_F}{q}(a_--a_+-\sqrt{a_+^2-1}-\sqrt{a_-^2-1}) , \tag{3.7}$$

where

$$a_\pm=\frac{\omega\pm\omega_n+i\delta}{qv_F}\pm\frac{q}{2k_F} , \tag{3.8}$$

with

$$\omega_n=E_n-E_0 . \tag{3.9}$$

The quasiparticle energies E_n are calculated in the LDA.

The effective perturbing potential $H'(q)$ in Eq. (3.3) is given by

$$H'(q)=eDz+\Delta V_H(q,z)+\Delta V_{\rm xc}(q,z) . \tag{3.10}$$

The change $\Delta V_H(q,z)$ of the Hartree potential is given by the solution of Poisson's equation with the change in the charge density Δn as the source term

$$\nabla^2(\Delta V_H(q,z)e^{i\mathbf{q}\cdot\mathbf{r}})=-\frac{4\pi e^2}{\epsilon_0}\Delta n(q,z)e^{i\mathbf{q}\cdot\mathbf{r}} , \tag{3.11}$$

which is solved to give

$$V_H(q,z)=\frac{2\pi e^2}{\epsilon_0 q}\int_{-\infty}^{\infty}dz'e^{-q|z-z'|}\Delta n(q,z') . \tag{3.12}$$

For the change $\Delta V_{\rm xc}(q,z)$ of the exchange-correlation potential we have

$$\Delta V_{\rm xc}(q,z)=\frac{\partial V_{\rm xc}}{\partial n(z)}\Delta n(q,z) , \tag{3.13}$$

where the exchange-correlation potential $V_{\rm xc}$ is taken in the LDA approximation in the parametrized form suggested by Hadin and Lundqvist [Eq. (2.2)]. As we mentioned above, $\Delta V_H(q,z)$ takes into account resonance screening effect whereas $\Delta V_{\rm xc}(q,z)$ is the excitonic correction.

The induced charge density, because of the perturbation, induces a current, which through the continuity equation becomes

$$\frac{d}{dz}j(q,z)=-(-i\omega)(-e)\Delta n(q,z) \tag{3.14}$$

or

$$j(q,z)=i\omega e\int_{-\infty}^{z}dz'\Delta n(q,z') . \tag{3.15}$$

Substituting for $\Delta n(q,z)$ from Eq. (3.3) we finally get for the induced current

$$j(q,z)=2i\omega eN_S\sum_{n>0}\Pi_n(q,\omega)\langle n|H'(q)|0\rangle \times\int_{-\infty}^{z}dz'\zeta_n(z')\zeta_0(z') \ . \quad (3.16)$$

The induced current is related to the induced polarization $P(q,z)=(i/\omega)j(q,z)$ and the total electric field in the z direction of confinement is given by

$$E(q,z)=D-\frac{4\pi i}{\omega}j(q,z) \ . \quad (3.17)$$

The absorption of radiation per unit area is

$$\mathcal{P}\sim\tfrac{1}{2}\mathrm{Re}\int_{-\infty}^{\infty}dzj(q,z)E^*(q,z) \ , \quad (3.18)$$

and using Eq. (3.17) we get

$$\mathcal{P}\sim\tfrac{1}{2}\mathrm{Re}\int_{-\infty}^{\infty}dzj(q,z)D \ . \quad (3.19)$$

We want to calculate the two-dimensional conductivity[1] which is the response function of the system. In the linear-response theory we have[1]

$$j(q,z)=\sigma_{zz}(q,\omega)\delta(z)D \ , \quad (3.20)$$

where the electron layer is replaced by a polarizable sheet at $z=0$. In the language of the diagrammatic perturbation theory $\sigma_{zz}(q,\omega)$ in Eq. (3.20) corresponds to the reducible response function of the system as discussed in Secs. I and II A. With the use of Eq. (3.20) the absorption per unit area becomes proportional to

$$\mathcal{P}\sim\tfrac{1}{2}\mathrm{Re}\sigma_{zz}(q,\omega)D^2 \ , \quad (3.21)$$

whereas, the conductivity becomes

$$\sigma_{zz}(q,\omega)=\frac{1}{D}\int_{-\infty}^{\infty}dzj(q,z) =\frac{-2i\omega eN_S}{D}\sum_{n>0}z_{n0}\Pi_n(q,\omega)\langle n|H'(q)|0\rangle \quad (3.22)$$

with

$$z_{n0}=\int_{-\infty}^{\infty}dzz\zeta_n(z)\zeta_0(z) \ . \quad (3.23)$$

The next step is to calculate the matrix element $\langle n|H'(q)|0\rangle$ of the effective perturbation $H(q)$ given by Eq. (3.10). It is

$$\langle n|H'(q)|0\rangle=eDz_{n0}+\langle n|\Delta V_H(q,z)|0\rangle +\langle n|\Delta V_{\mathrm{xc}}(q,z)|0\rangle \ . \quad (3.24)$$

Using Eq. (3.12) for the Hartree term, we get

$$\langle n|\Delta V_H(q,z)|0\rangle=-2N_S\sum_{m>0}\frac{4\pi e^2}{\epsilon_0}\Pi_m(q,\omega)S_{nm}(q) \times\langle m|H'(q)|0\rangle \quad (3.25)$$

with

$$S_{nm}(q)=\frac{1}{2q}\int_{-\infty}^{\infty}dz\zeta_n(z)\zeta_0(z) \times\int_{-\infty}^{\infty}dz'e^{-q|z-z'|}\zeta_n(z')\zeta_0(z') \ . \quad (3.26)$$

For the exchange-correlation matrix element we have,

$$\langle n|\Delta V_{\mathrm{xc}}(q,z)|0\rangle=-2N_S\sum_{m>0}\Pi_m(q,\omega)\langle m|H'(q)|0\rangle \times\int_{-\infty}^{\infty}dz\zeta_n(z)\zeta_m(z)\zeta_0^2(z) \times\frac{\partial V_{\mathrm{xc}}}{\partial n} \ . \quad (3.27)$$

Using Eqs. (3.24)–(3.27) we finally get

$$\langle n|H'(q)|0\rangle=eDz_{n0}-2N_S\sum_{m>0}\Pi_m(q,\omega)\left[\frac{4\pi e^2}{\epsilon_0}S_{nm}(q)\int_{-\infty}^{\infty}dz\zeta_n(z)\zeta_m(z)\zeta_0^2(z)\frac{\partial V_{\mathrm{xc}}}{\partial n}\right]\langle m|H'(q)|0\rangle \ , \quad (3.28)$$

If we now define the matrices

$$\alpha_{nm}(q)=2N_S\frac{4\pi e^2}{\epsilon_0}S_{nm}(q)\left[\frac{1}{\omega_n}\frac{1}{\omega_m}\right]^{1/2} \quad (3.29)$$

and

$$\beta_{nm}=-2N_S\left[\frac{1}{\omega_n}\frac{1}{\omega_m}\right]^{1/2} \times\left[\int_{-\infty}^{\infty}dz\zeta_n(z)\zeta_m(z)\zeta_0^2(z)\frac{\partial V_{\mathrm{xc}}}{\partial n}\right] , \quad (3.30)$$

and set

$$u_n(q,\omega)=\frac{1}{eD}(2m)^{1/2}\frac{\Pi_n(q,\omega)}{(\omega_n)^{1/2}}\langle n|H'(q)|0\rangle \ , \quad (3.31)$$

we finally get the matrix equation

$$\sum_{m>0}\{A_{nm}(q,\omega)-\omega^2\delta_{nm}\}u_{nm}(q,\omega)=(2m\omega_n)^{1/2}z_{n0} \ , \quad (3.32)$$

where

$$A_{nm}(q,\omega)=\left[\frac{\omega_n}{\Pi_n(q,\omega)}+(\omega)^2\right]\delta_{nm} +\omega_n(\alpha_{nm}(q)-\beta_{nm})\omega_m \quad (3.33)$$

and ω_n is given by Eq. (3.9). With the help of Eqs. (3.32) and (3.33), Eq. (3.22) for the conductivity finally becomes (we have put the $\hbar$ back in this equation)

$$\sigma_{zz}(q,\omega)=N_S e^2(-i\omega)\left[\frac{\hbar^2}{m}\right] \times \sum_{n>0}\sum_{m>0} u_n(q,\omega)[A_{nm}(q,\omega) -(\hbar\omega)^2\delta_{nm}]u_m(q,\omega) . \tag{3.34}$$

The above equation is our final formula for the conductivity of the confined electron gas. Unfortunately it is not very useful for practical purposes as it stands, since the matrix $A_{nm}(q,\omega)$ in Eq. (3.34) is nondiagonal and we sum over all (in principle infinite) subband indices n and m. We therefore define a matrix U such that $\tilde{A}=U^{-1}AU$ is diagonal. Because A is symmetric, U is an orthogonal matrix. After some cumbersome matrix algebra we can rewrite Eq. (3.34) in the simpler form,

$$\sigma_{zz}(q,\omega)=\frac{N_S e^2}{m}(-i\omega)\sum_{n>0}\frac{\tilde{f}_n(q,\omega)}{\tilde{\omega}_n^2-\omega^2-2i\omega/\tau} , \tag{3.35}$$

where

$$\hbar\tilde{\omega}_n=(\tilde{A}_{nn}(q,\omega))^{1/2} \tag{3.36}$$

and the oscillator strength $\tilde{f}_n(q,\omega)$ is given by

$$\tilde{f}_n(q,\omega)=\left[\sum_{m>0}\left[\frac{2m}{h^2}\hbar\omega_m\right]^{1/2} z_{m0}U_{mn}(q,\omega)\right]^2 . \tag{3.37}$$

In Eq. (3.37) we have introduced a phenomenological relaxation time τ which arises from impurity scattering in the system. The resonance occurs at the frequencies $\omega=\tilde{\omega}_n$.

If we now concentrate on the situation where the radiation frequency ω is close to $\tilde{\omega}_n$ we can neglect contributions from other subbands. This two-subband approximation is a very good approximation in high-mobility samples, where the width of the resonance is narrower than the intersubband spacing. In this case we can write Eq. (3.35) as

$$\sigma_{zz}(q,\omega)=\frac{(-i)N_S e^2\omega}{m}\left[\frac{\tilde{f}_n(q,\omega)}{\tilde{\omega}_n^2-\omega^2-2i\omega/\tau}\right] , \tag{3.38}$$

with

$$\tilde{f}_n(q,\omega)=\frac{2m}{\hbar^2}\hbar\omega_n z_{n0}^2 . \tag{3.39}$$

The dispersion relation of the collective intersubband modes in this case is given by the solutions of the equation

$$1+\Pi_n(q,\omega)\hbar\omega_n[\alpha_{nn}(q)-\beta_{nn}]=0 . \tag{3.40}$$

In the rest of this paper we are going to study in detail solutions of Eq. (3.40). When we are out of resonance contributions from other subbands may be important, especially in wide quantum wells and at high densities. In this case Eq. (3.35) should be used.

We consider briefly the $q\to 0$ limit of our results. From Eq. (3.6) we have for the $q\to 0$ limit of $\Pi_n(q,\omega)$,

$$\Pi_n(q,\omega)=\frac{\omega_n}{\omega^2-\omega_n^2} +\frac{1}{2m}\left[\frac{\omega^2+\omega_n^2}{(\omega^2-\omega_n^2)^2}+\left[\frac{\pi N_S\omega_n}{m}\right]\frac{3\omega^2+\omega_n^2}{(\omega^2-\omega_n^2)^3}\right] \times q^2+0(q^4) . \tag{3.41}$$

From Eqs. (3.29) and (3.30) we also have

$$\alpha_{nm}(q)=\left[\frac{2N_S}{\omega_n}\right](a_{nn}^{(0)}-a_{nn}^{(1)}q+a_{nn}^{(2)}q^2-a_{nn}^{(3)}q^3+\cdots) \tag{3.42}$$

and

$$\beta_{nm}=\left[\frac{2N_S}{\omega_n}\right]\lambda_{nn} , \tag{3.43}$$

with

$$a_{nm}^{(\nu)}=\frac{4\pi e^2}{\varepsilon_0}\frac{1}{\nu!}\int_0^\infty dz\zeta_n(z)\zeta_0(z) \times\int_0^\infty dz'\zeta_n(z')\zeta_0(z') \times(|z+z'|^{\nu+1}-|z-z'|^{\nu+1}) \tag{3.44}$$

and

$$\lambda_{nn}=-2\int_{-\infty}^{\infty}dz\zeta_n(z)\zeta_m(z)\xi_0^2(z)\left[\frac{\partial V_{xc}}{\partial n}\right] . \tag{3.45}$$

Using now Eqs. (3.41), (3.42), and (3.43) in Eq. (3.40), we finally get for the intersubband charge-density dispersion in the limit of long wavelengths up to order q^2,

$$\omega_p^2=\omega_n^2+2N_S\omega_n(a_{nn}^{(0)}-\lambda_{nn})-2N_S\omega_n a_{nn}^{(1)}q +\left[2N_S\omega_n a_{nn}^{(2)}+\frac{\omega_n+N_S(a_{nn}^{(0)}-\lambda_{nn})}{m}+\frac{2\pi[2\omega_n+3N_S(a_{nn}^{(0)}-\lambda_{nn})]}{4m^2(a_{nn}^{(0)}-\lambda_{nn})}\right]q^2-0(q^3) . \tag{3.46}$$

The above formula is in agreement with Ando's result for $q=0$ and with Tselis and Quinn[20] for finite q. It is also very similar to Eq. (1.6) derived in Sec. I, with the only difference being that we now include exchange and correlation effects and calculate single-particle wave functions and energies self-consistently. Note that the approach we followed to derive Eq. (3.46) is very different from that in Sec. I where we explicitly calculate diagrams in perturbation theory. From Eq. (3.46) we see that the effect of the exchange and correlation, even within our LDA theory,

persists to all orders in q. To avoid misunderstanding we mention that in the numerical results we present in the next section, we are using the full formula (3.40) which incorporates the full q dependence and not just the leading-order corrections.

It is worthwhile to point out the connection between results in this section with those in Secs. II B and I B which were obtained on the basis of a diagrammatic theory. Equation (3.40) for the collective modes in this section are identical to those derived for the intersubband charge-density excitation in Sec. II B (and those obtained within the RPA in Sec. I B except that $\beta_{nn}=0$ for the RPA calculation because there is no vertex correction). The α and the β terms of Eq. (3.40) correspond, respectively, to the V^{1010} direct Coulomb term and the U_{xc}^{1010} excitonic vertex correction term in Eq. (2.13). The α and the β corrections (i.e., the direct Coulomb and the vertex correction) have been referred to as the depolarization shift and the excitonic correction, respectively.

IV. RESULTS

In our study, we assume occupation only of the lowest subband in the well and consider only excitations between the ground and the first excited subbands.

We start presenting our numerical results by showing in Fig. 5 as a function of electron density the long-wavelength charge- and spin-density excitation energies. We also show the quasiparticle energy difference between the lowest two subbands in various approximations: (1) neglecting other electrons in the well (bare subband separation), (2) considering interactions with other electrons in the Hartree approximation, and finally, (3) including exchange and correlation effects in LDA. These results are for the parabolic quantum well of Fig. 4.

The coincidence of the bare subband separation with the long-wavelength charge-density excitation, with and without vertex corrections, throughout the density range we studied shows how well the generalized Kohn's theorem is obeyed in our parabolic system. The small deviation of the collective charge-density excitation energy from the bare subband separation at high densities arises from the deviation at the well edges of our realistic well from perfect parabolicity. These deviations from perfect parabolicity are more important at higher densities because the electron gas better "feels" the edge of the well at higher densities. We also see that exchange-correlation effects partly cancel contributions of the Hartree term and bring the subband separation closer to the bare one, in agreement with previous work on the electronic structure of GaAs-based quantum wells. It is worth noting in Fig. 5 that at low densities (we investigate densities down to 8×10^{8} cm^{-2}) exchange-correlation effects become relatively more significant and bring the quasiparticle energy difference above the bare subband separation. We will soon see that this can have significant consequence[5] for the low-density collective-mode dispersion. At low densities the quasiparticle energy difference in the Hartree approximation becomes quantitatively almost identical to the spin-density excitation energy at zero wave vector because the vertex correction and the self-energy correction cancel each other. The spin-density excitations are not affected by the depolarization shift, which, therefore, is set equal to zero in their calculation [$\alpha_{nn}=0$ in Eq. (3.40)], and, at low densities, the Hartree term in the quasiparticle energy difference is not that important.

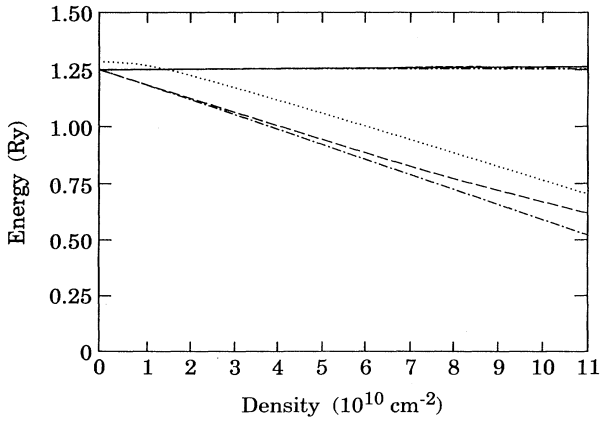

FIG. 5. Long-wavelength ($q=0$) charge-density excitation in both RPA and TDLDA (both are shown by the solid line, cannot be distinguished separately) and spin-density excitations (dashed-dotted) as a function of density. Also, the bare subband separation (dashed-dot-dot), subband separation in the Hartree approximation (dashed), and the LDA subband separation (dotted). The above results correspond to the parabolic well of Fig. 4.

In Fig. 6 we show the dispersion relation of intersubband plasmons (i.e., the charge-density excitations) arising from collective transitions between the two lowest subbands for the parabolic well of Fig. 4 as a function of wave vector for different electron densities in the well. We also plot the boundaries of the single-particle excitation spectrum given by $E_1-E_0\pm qv_F+q^2/2m$. We clearly see the minimum in the dispersion at experimentally accessible densities ($\sim10^{11}$ cm^{-2}) that we first encountered in our many-body RPA calculation of Sec. I. For the electron density of 1.1×10^{11} cm^{-2} the minimum is 0.5-meV deep and should be observable in resonant Raman-scattering experiments. As we decrease the density, the minimum becomes more shallow and the plasmon disappears into the particle-hole continuum at smaller wave vectors. At densities around 1.5×10^{10} cm^{-2} the quasiparticle energy difference for the lowest two subbands coincides with the bare subband separation (the Kohn mode) and we do not see any plasmons, since the collective modes is now completely (i.e., even at long wavelengths) inside the single-particle continuum. For our discussions, we consider this density as the boundary between the high- and the low-density regimes. As we decrease the density even further, the quasiparticle energy difference becomes *higher* than the plasmon energy and we recover the long-wavelength plasmon below the Landau continuum, which becomes Landau damped at finite wave vectors. An interesting feature that accompanies this behavior of the collective mode is that, as the quasiparticle energy difference crosses the bare subband

separation, a change in the curvature of the plasmon dispersion relation occurs. This could be attributed to the following. As is well known, the collective modes correspond to the coherent excitation of the system whereas the single-particle excitations are incoherent. As the single-particle excitation is only slightly above the collective mode, it "forces" the plasmon down in the familiar level repulsion manner. In other words, at resonance, the coherent mode tends to become more favorable than the incoherent one, when both are close in energy. Even though this change in curvature of the collective mode is small, it is accompanied by a large variation in the critical plasmon wave vector for Landau damping as we vary the electron density. Therefore, we believe

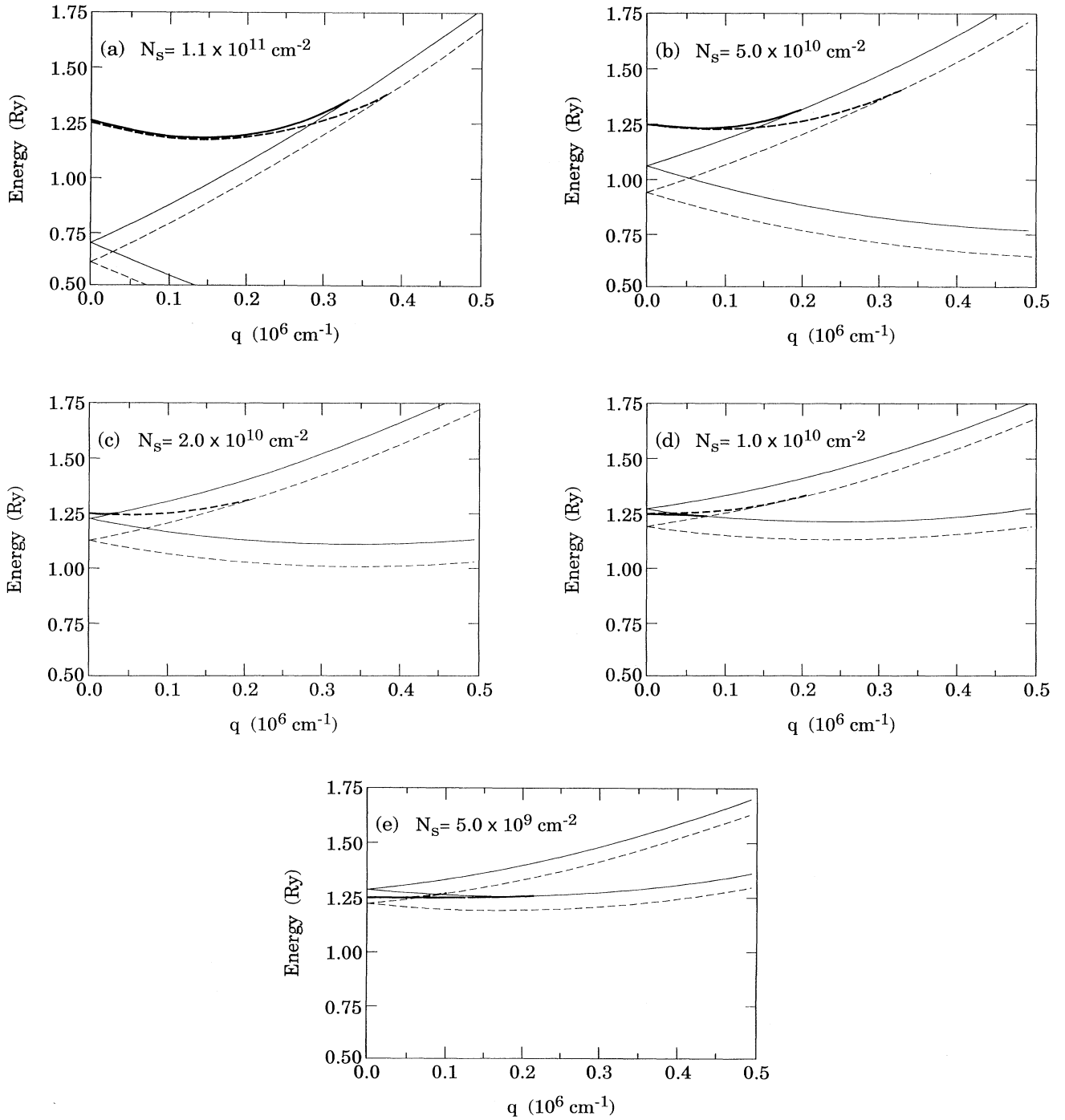

FIG. 6. Dispersion relation of the collective intersubband charge-density excitation (thick lines) between the lowest two subbands of the parabolic well of Fig. 4 as a function of wave vector for various densities as shown. We show results in RPA (dashed lines) and in TDLDA (solid lines). The boundaries of the corresponding single-particle excitation continua are also shown (thin lines).

that experiments probing simultaneously the energy and the wave vector of the collective mode can detect this interesting many-body effect. Resonant Raman-scattering technique, for example, is particularly well suited to study this phenomenon, which is a direct manifestation of the interplay between the single particle and the collective excitation spectra of a confined electron gas. It is also interesting to note that the RPA gives results quantitatively similar to TDLDA, particularly at small wave vectors. We also see that, although RPA and TDLDA give similar results for small wave vectors, they predict quite different critical wave vectors for the onset of the Landau damping of the intersubband plasmon.

In Fig. 7 we show our TDLDA results for the intersubband spin-density excitation spectrum associated with the transitions between the lowest two subbands in the parabolic well of Fig. 4. From our results in Fig. 7 we see that as we decrease the electron density the curvature of the spin-density dispersion changes gradually whereas the maximum wave vector for which the mode is well defined increases slightly. Our results can be easily tested experimentally using Raman scattering in the cross-polarization configuration.

For the sake of comparison with the parabolic well results, we show in Fig. 8 the intersubband plasmon dispersion for a 400-Å-wide square well. In the same figure we also show the boundaries of the single-particle excitation continuum defined by $E_1 - E_0 \pm q v_F + q^2/2m$. We see that at moderate densities we do get a minimum in the dispersion relation as deep as the one found for the parabolic well. As we decrease the density, the minimum becomes shallower, and, in general, we get the same qualitative behavior as in the case of parabolic wells. If we decrease the width of the square well down to 200 Å, we do not get any appreciable dispersion minima (Fig. 9). These results make clear that the minimum we predict in the dispersion relation of intersubband plasmons at finite wave vectors is a general characteristic of the confined electron gas independent of the shape of the well provided the well is wide enough. The depth of the minimum and the form of the dispersion are determined by the details of the competition between the strength of the interaction which tends to reduce the energy of the system, and the strength of the confinement which tends to increase the energy of the system.

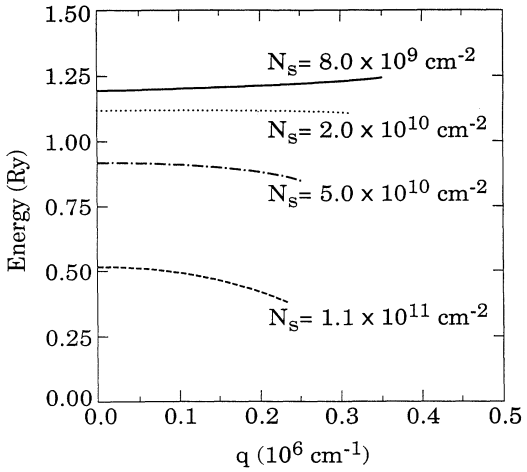

FIG. 7. Dispersion relation of the spin-density excitations as a function of wave vector for different densities. We plot the dispersion up to the maximum wave vector for which the mode is well defined. Results correspond to the parabolic well of Fig. 4.

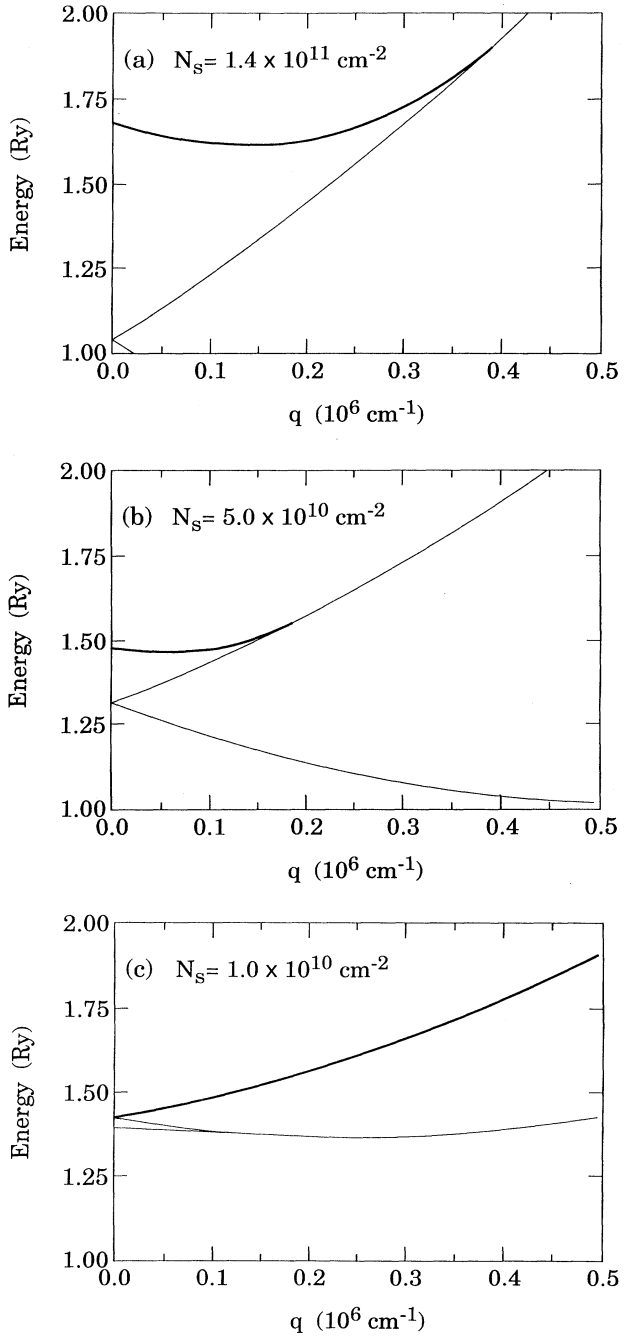

FIG. 8. Dispersion relation of the TDLDA collective charge-density excitations (thick lines) as a function of wave vector for different densities in a square well (width 400 Å, height 75 Ry). Thin lines correspond to the boundaries of the single-particle excitation continuum.

Finally, in Figs. 10–13 we present results for the calculated intersubband optical absorption line shapes in the parabolic quantum well of Fig. 4 with a mobility 100 000 $cm^2 V^{-1} s^{-1}$ [which determines the relaxation-time parameter τ in Eq. (3.37)]. At zero wave vectors we get only one absorption peak at the bare subband separation

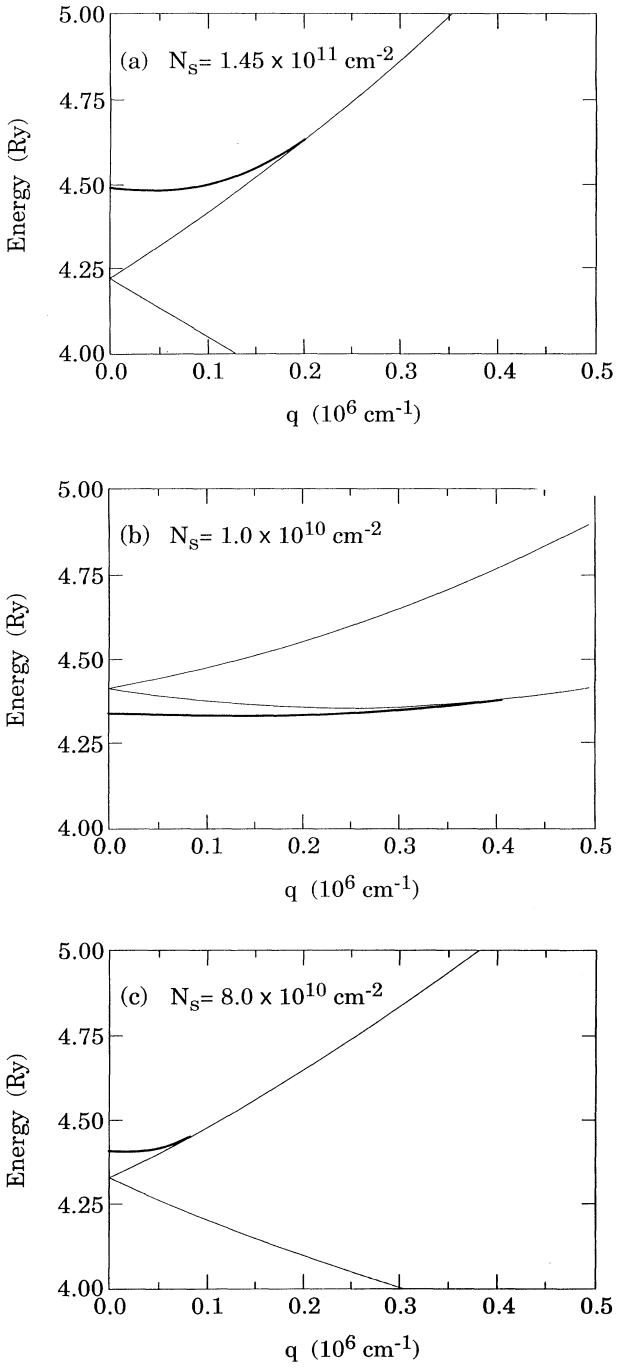

FIG. 9. Dispersion relation of the TDLDA collective charge-density excitations (thick lines) as a function of wave vector for different densities in a square well (width 200 Å, height 75 Ry). Thin lines correspond to the boundaries of the single-particle excitation continuum.

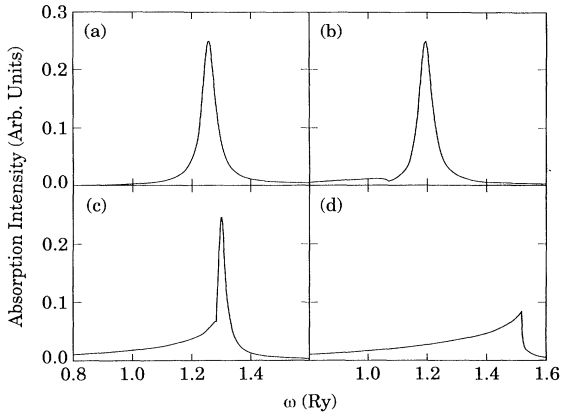

FIG. 10. Line shapes of the TDLDA-calculated optical-absorption spectra in the parabolic quantum well of Fig. 4 have a mobility of 100 000 $cm^2 V^{-1} s^{-1}$ and an electron density of 1.1×10^{11} cm^{-2} as a function of frequency for different wave vectors expressed in dimensionless atomic units (by multiplying them with $a_B = \hbar^2 \varepsilon_0 / me^2 = 98.7$ Å) $qa_B = 0.001$ (a); 0.2 (b); 0.3 (c); and 0.4 (d).

(the Kohn mode). In this case, the Kohn mode saturates the oscillator sum rule and is the only peak in the optical absorption. At finite wave vectors, we start getting small additional contributions from single-particle excitations which show up in the absorption line shape as a small shoulder to the left (right) of the plasmon peak at high (low) densities, respectively, but at small wave vectors the intersubband plasmon is still the dominant mode. The position of the plasmon peak, of course, follows the dispersion relation presented earlier (Fig. 6). At large wave vectors the plasmon peak merges with the single-particle excitation continuum (i.e., the plasmon becomes Landau damped) and we get a broad structure in absorption. At lower densities (Figs. 12 and 13) the plasmon merges with the single-particle continuum at lower wave vectors. From our results we see that experiments that measure absorption at finite wave vectors can detect signatures from both plasmons and single-particle excitations and, therefore, can be used to study the many-body

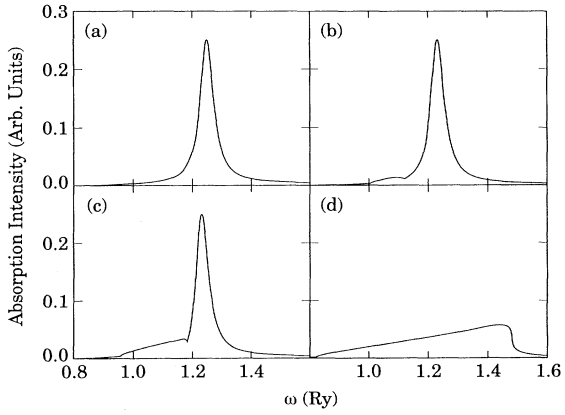

FIG. 11. The same as in Fig. 10 for $N_S = 5 \times 10^{10}$ cm^{-2}, and for $qa_B = 0.001$ (a); 0.05 (b); 0.1 (c); and 0.3 (d).

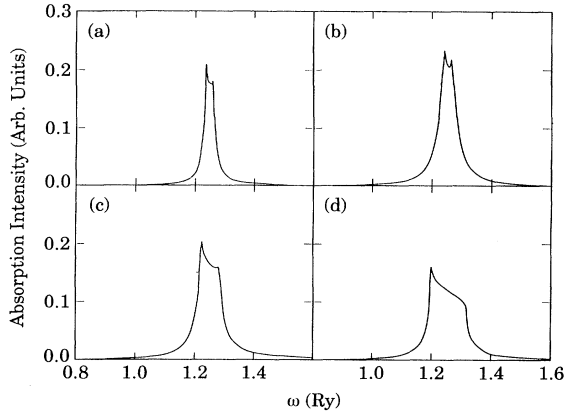

FIG. 12. The same as in Fig. 10 for $N_S = 1.5 \times 10^{10}$ cm^{-2}, and for $qa_B = 0.02$ (b); 0.05 (c); 0.1 (d). (a) corresponds to $qa_B = 0.02$, but a purer sample with a higher mobility of 200 000 cm^2 v^{-1} s^{-1}.

phenomena associated with the interplay between the collective and the single-particle excitations discussed above.

The most interesting aspect of the absorption spectra shown in Figs. 10–13 is the level splitting phenomenon most apparent in Fig. 12, which arises from a resonant many-body coupling between intersubband single-particle and collective excitations. At low electron densities ($\sim 1-2\times 10^{10}$ cm^{-2}) and wide enough wells (we have checked to ensure that the resonant level splitting occurs also in square-well structures around the same electron density regime), the resonant coupling produces a level splitting (Fig. 12) in the far-infrared absorption spectra even at rather long wavelengths ($q \approx 1-2\times 10^4$ cm^{-1}) because the collective charge density excitation is almost degenerate with the single-particle Landau continuum even at long wavelengths around this density regime. Note that above this critical density ($\sim 1.5\times 10^{10}$ cm^{-2}), the intersubband charge-density mode behaves as the usual plasmon mode lying above the single-particle Landau continuum whereas below this density vertex correction pushes the collective mode below the Landau continuum and we have a strange situation where the plasmon lies below the single-particle continuum. In the latter situation, it is perhaps more appropriate to think of the intrasubband charge density excitation to be a collective coupled plasmon-exciton mode—it is a plasmon in the sense that it is the pole of a reducible response function, but it is also in some sense a many-body exciton because the vertex correction arising from strong intersubband electron-hole interaction pushes the energy of the excitation below the single-particle continuum, giving it somewhat of a bound state nature. We want to emphasize that this resonant level splitting phenomenon is a pure many-body phenomenon, arising entirely due to the vertex correction on the polarizability inherent in the TDLDA—in the RPA, the intersubband charge-density excitation must always lie above the single-particle continuum as is obvious from our results in Fig. 6. We believe that this predicted level splitting phenomenon should be observable in both far-infrared absorption and inelastic light scattering experiments at low temperatures—our theoretical calculations use realistic system parameters including a rather conservative estimate of the impurity broadening which would tend to wash out the resonance effect.

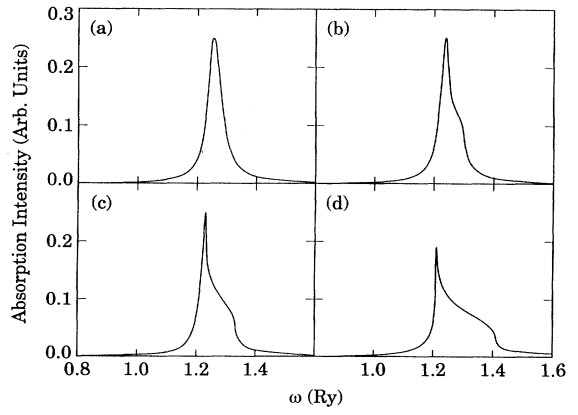

FIG. 13. The same as in Fig. 10 for $N_S = 10^{10}$ cm^{-2}, and for $qa_B = 0.001$ (a); 0.05 (b); 0.1 (c); and 0.2 (d).

We note that the real part of the conductivity (which is proportional to the absorption per unit area) is also proportional to the imaginary part of the density response function which is essentially the dynamical structure factor of the system. For the two-dimensional electron systems the dynamical structure factor $S(q,\omega)$ is related to the conductivity (response function) through the formula

$$S(q,\omega) = \frac{2q}{\pi e^2 \omega d} \mathrm{Re}\sigma_{zz}(q,\omega) , \tag{4.1}$$

where d is of the order of the thickness of the electron layer. From Eq. (4.1) we expect Raman-scattering experiments, which basically probe the dynamical structure factor of the many-body system, to reveal similar qualitative features as that shown in Figs. 10–13. Thus, we can take the numerical results of Figs. 10–13 as giving the Raman-scattering spectra (up to an overall scale factor) associated with the intersubband charge-density excitations as well.

V. SUMMARY

In this paper we develop a zero-temperature theory for the intersubband elementary excitation spectra of wide parabolic (and square) quantum wells in the extreme quantum limit when only the lowest subband is occupied in the ground state of the system. We use the self-consistent TDLDA theory where the electronic structure of the system is obtained by self-consistently solving the LDA Kohn-Sham equation and the elementary excitations are obtained from the poles of the suitable intersubband polarizability functions which are themselves calculated in a self-consistent-field linear-response calculation using the LDA subband wave functions and energies. We have also obtained the spectral weight of the elementary excitation spectra by calculating the dynamical conductivity, or equivalently, the dynamical structure factor of the system. In particular, we calculate the intersub-

band optical absorption associated with far-infrared spectroscopy and the inelastic-light-scattering spectra associated with Raman-scattering spectroscopy. We use realistic quantum well configurations for our calculations. We concentrate on wide parabolic (and, square) quantum wells and on low two-dimensional electron densities in the system. We find that for wide enough wells, there is an interesting and experimentally observable shallow minimum in the intersubband collective charge-density excitation (i.e., plasmon) mode at a finite value of the in-plane wave vector. This minimum is not a many-body effect (in the sense a roton minimum is in the case of superfluids or quantum Hall liquids), and exists both in the RPA and the TDLDA theory. We argue that this intersubband plasmon dispersion minimum has the same origin as the negative surface-plasmon dispersion[27] in metal surfaces and arises from a competition between confinement and nonlocal (i.e., finite wave vector) response. Our most significant theoretical finding is a subtle many-body coupling between the intersubband single-particle continua and the intersubband charge-density excitations which is a direct result of keeping the excitonic vertex corrections in the theory and shows up only in the TDLDA theory (and, *not* in the RPA). This coupling causes even the long-wavelength intersubband plasmon mode to be Landau damped at some critical electron density ($\sim 1-2\times 10^{10}$ cm^2) and, below this critical density, the intersubband plasmon lies *below* the quasiparticle Landau continuum because the excitonic vertex correction actually becomes larger in magnitude than the depolarization shift. Around the critical density, the plasmon is strongly resonantly coupled to the Landau quasiparticle continuum, leading to an experimentally observable line splitting of the intersubband charge-density excitation peak. This predicted many-body resonant plasmon line-splitting phenomenon should be observable both in inelastic light scattering and far-infrared optical spectroscopies. We provide detailed numerical results for the calculated intersubband charge-density, spin-density, and quasiparticle excitation spectra, critically comparing TDLDA and RPA theoretical results so that one can estimate the magnitudes of exchange-correlation corrections on the elementary excitation spectra of GaAs-based two-dimensional structures. We also provide some comparison between parabolic well and square-well structures.

We have also provided in this article the unified formalism for RPA and TDLDA theories of the elementary excitation spectra in semiconductor quantum wells. In particular, we have developed both the theories from a unified many-body diagrammatic formalism as well as from a self-consistent-field equation-of-motion approach. The TDLDA theory includes LDA exchange-correlation corrections both in the subband structure calculation and in the self-consistent linear-response calculation whereas RPA does not (of course, both calculations must include the Hartree correction self-consistently). In the many-body language, the RPA includes only the Hartree self-energy correction in the subbands whereas the TDLDA includes both Hartree and LDA exchange-correlation self-energies. In addition, the irreducible polarizability (whose poles define the spin density excitations) in the RPA is only the (Hartree-corrected) bare bubble whereas in the TDLDA it is the ladder polarizability diagrams. The ladder vertex equation for the irreducible polarizability can be easily solved because LDA makes the drastic approximation of taking the exchange-correlation potential to be static and short-ranged (in fact, zero-range δ-function-like). The reducible polarizability (whose poles define the charge density excitations) is given by the sum of the "ring" diagrams in both the approximations (with each ring being LDA vertex corrected by the ladders in TDLDA and each ring being bare in RPA).

ACKNOWLEDGMENT

This work was supported by the US-ARO and the US-ONR.

*Present address: Instituut-Lorentz for Theoretical Physics, University of Leiden, Postbus 9506, 2300 RA Lieden, The Netherlands.

[1]T. Ando, A. B. Fowler, and F. Stern, Rev. Mod. Phys. **54**, 437 (1982), and references therein.

[2]D. Heitmann, Surf. Sci. **170**, 332 (1988), and references therein; A. Pinczuk and G. Abstreiter, in *Light Scattering in Solids V*, edited by M. Cardona and G. Guntherodt (Springer-Verlag, Berlin, 1989), and references therein.

[3]K. Karrai, H. D. Drew, M. W. Lee, and M. Shayegan, Phys. Rev. B **39**, 1426 (1989); K. Karrai, X. Ying, H. D. Drew, and M. Shayegan, *ibid.* **40**, 12 020 (1989).

[4]K. Karrai, M. Stopa, X. Ying, H. D. Drew, S. Das Sarma, and M. Shayegan, Phys. Rev. B **42**, 9732 (1990).

[5]A. Wixforth, M. Sundaram, J. H. English, and A. C. Gossard, Surf. Sci. **267**, 523 (1992).

[6]A. Wixforth, M. Sundaram, K. Ensslin, J. H. English, and A. C. Gossard, Phys. Rev. B **43**, 10 000 (1991); M. Kaloudis, K. Ensslin, A. Wixforth, M. Sundaram, J. H. English, and A. C. Gossard, *ibid.* **46**, 12 469 (1992).

[7]P. R. Pinsukanja, E. Yuh, E. L. Asmar, E. G. Gwinn, M. Sundaram, and A. C. Gossard, Phys. Rev. B **46**, 7284 (1992).

[8]L. Brey, N. F. Johnson, and B. I. Halperin, Phys. Rev. B **40**, 10 647 (1989). See also Q. P. Li, K. Karrai, S. K. Yip, S. Das Sarma, and H. D. Drew, *ibid.*, **43**, 5151 (1991).

[9]L. Brey, J. Dempsey, N. F. Johnson, and B. I. Halperin, Phys. Rev. B **42**, 1240 (1990); L. Brey, N. F. Johnson, and J. Dempsey, *ibid.* **42**, 2886 (1990); M. P. Stopa and S. Das Sarma, *ibid.* **45**, 8526 (1992).

[10]M. P. Stopa and S. Das Sarma, Phys. Rev. B **40**, 10 048 (1989); **47**, 2122 (1993); L. Brey, *ibid.* **44**, 3772 (1991); J. Dempsey and B. I. Halperin, *ibid.* **45**, 3902 (1992).

[11]S. Das Sarma, Phys. Rev. B **29**, 2334 (1984).

[12]J. K. Jain and S. Das Sarma, Phys. Rev. B **36**, 5949 (1987); Surf. Sci. **196**, 466 (1988).

[13]S. Das Sarma, Appl. Surf. Sci. **11/12**, 535 (1982).

[14]B. Vinter, Phys. Rev. B **15**, 3947 (1977); **13**, 4447 (1976); F. J. Ohkawa, Surf. Sci. **58**, 326 (1976); S. Das Sarma and R. Jala-

bert, Phys. Rev. B **40**, 9723 (1989); S. Das Sarma, R. Jalabert, and S. R. E. Yang, *ibid.* **41**, 8288 (1990); I. K. Marmorkos and S. Das Sarma, *ibid.* **44**, 3451 (1991).

[15]S. Das Sarma and B. Vinter, Phys. Rev. B **23**, 6832 (1981); **26**, 960 (1982); **28**, 3639 (1983).

[16]S. Das Sarma, R. K. Kalia, M. Nakayama, and J. J. Quinn, Phys. Rev. B **24**, 7181 (1981).

[17]J. C. Ryan, Phys. Rev. B **43**, 12 406 (1991); D. Gammon, B. V. Shanabrook, J. C. Ryan, D. S. Katzer, and M. J. Yang, Phys. Rev. Lett. **68**, 1884 (1992).

[18]S. L. Chuang, M. S. C. Luo, S. Schmitt-Rink, and A. Pinczuk, Phys. Rev. B **46**, 1897 (1992).

[19]T. Ando, Z. Phys. B **26**, 263 (1977); T. Ando and S. Mori, J. Phys. Soc. Jpn. **47**, 1518 (1979); S. Katayama and T. Ando, *ibid.* **54**, 1615 (1985).

[20]A. Tselis and J. J. Quinn, Phys. Rev. B **29**, 3318 (1984); G. Eliasson, P. Hawrylak, and J. J. Quinn, *ibid.* **35**, 5569 (1987); R. D. King-Smith and J. C. Inkson, *ibid.* **33**, 5489 (1986).

[21]J. C. Ryan, Phys. Rev. B **43**, 4499 (1991); D. Gammon, B. V. Shanabrook, J. C. Ryan, and D. S. Katzer, *ibid.* **41**, 12 314 (1990).

[22]R. O. Jones and O. Gunnarsson, Rev. Mod. Phys. **61**, 689 (1989); A. R. Williams and U. von Barth, in *Theory of the Inhomogeneous Electron Gas,* edited by S. Lundqvist and N. H. March (Plenum, New York, 1983).

[23]L. Hedin and B. I. Lundqvist, J. Phys. C **4**, 2064 (1971).

[24]F. Stern and S. Das Sarma, Phys. Rev. B **30**, 840 (1984).

[25]W. Kohn and L. J. Sham, Phys. Rev. **140**, A1133 (1965).

[26]H. Ehrenreich and M. H. Cohen, Phys. Rev. **115**, 786 (1959).

[27]P. J. Feibelman, Phys. Rev. B **9**, 5077 (1974); A. Eguiluz, J. J. Quinn, and S. C. Ying, *ibid.* **11**, 2118 (1975); A. J. Bennett, *ibid.* **1**, 203 (1970).